Autonomous Synchronous Rectifier for Heart Pump Applications

Bob Wang, Aiguo Patrick Hu
Department of Electrical and Computer Engineering
The University of Auckland
Auckland, New Zealand
bwan033@aucklanduni.ac.nz; a.hu@auckland.ac.nz

David Budgett
Auckland Bioengineering Institute
Telemetry Research Limited
Auckland, New Zealand
d.budgett@auckland.ac.nz

***Abstract*— In order to reduce the power loss and associated temperature rise in the implanted side of the transcutaneous energy transfer system, the passive Schottky current doubler rectifier is replaced with an autonomous synchronous rectifier. Two options of driving the synchronous rectifier are proposed, passive autonomous operation and active gate drive using a buffer circuit. The synchronous rectifiers are found to have about 1.3% higher end-to-end efficiency compared to the Schottky only current doubler for the rated heart pump operational power of 10W.**

Keywords— Transcutaneous energy transfer; synchronous rectifier; push-pull; current doubler.

I. INTRODUCTION

Transcutaneous energy transfer (TET) offers a means of transmitting power across the skin from an exterior primary side circuitry to an implanted secondary side circuitry without using a percutaneous driveline penetrating the skin [1]. Eliminating this percutaneous driveline could significantly reduce the risk of infection [2]. In a TET system, apart from supplying the required power to drive the heart pump, one important challenge is to reduce the power loss at the implanted pickup circuit so as to reduce the heat generation and associated temperature rise. Because heart pumps are driven by a dc voltage, a rectifier is needed at the power pickup which is a source of power loss. Synchronous rectifiers can be used to replace the diode rectifiers to reduce the conduction losses of diodes, but complicated control circuits are often required. The zero crossings of the ac voltage was detected and a special ZVS (Zero Voltage Switching) circuit was designed to drive a push-pull synchronous rectifier [3], but the circuit was too complicated and power loss caused by additional circuits was high. Miura et al. [4, 5] also researched on push-pull synchronous rectifiers for TET systems using PLL control, again the system was complicated and overhead power loss became high. In this paper, a simple autonomous synchronous rectifier based on push-pull current doubler topology is introduced, and two drive options are proposed to lower the power loss of the implanted circuitry. The first drive option is fully self-sustained using passive components without the need of any auxiliary power supply and gate driver; while the second option uses a buffering circuit to improve the gate drive waveforms.

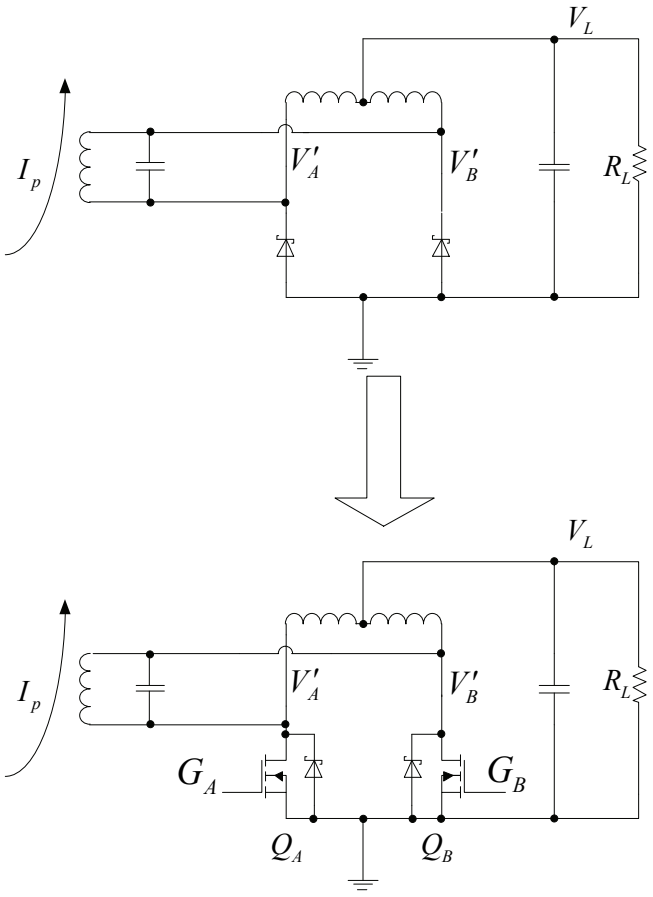

Fig. 1 Proposed main synchronous rectifier circuit

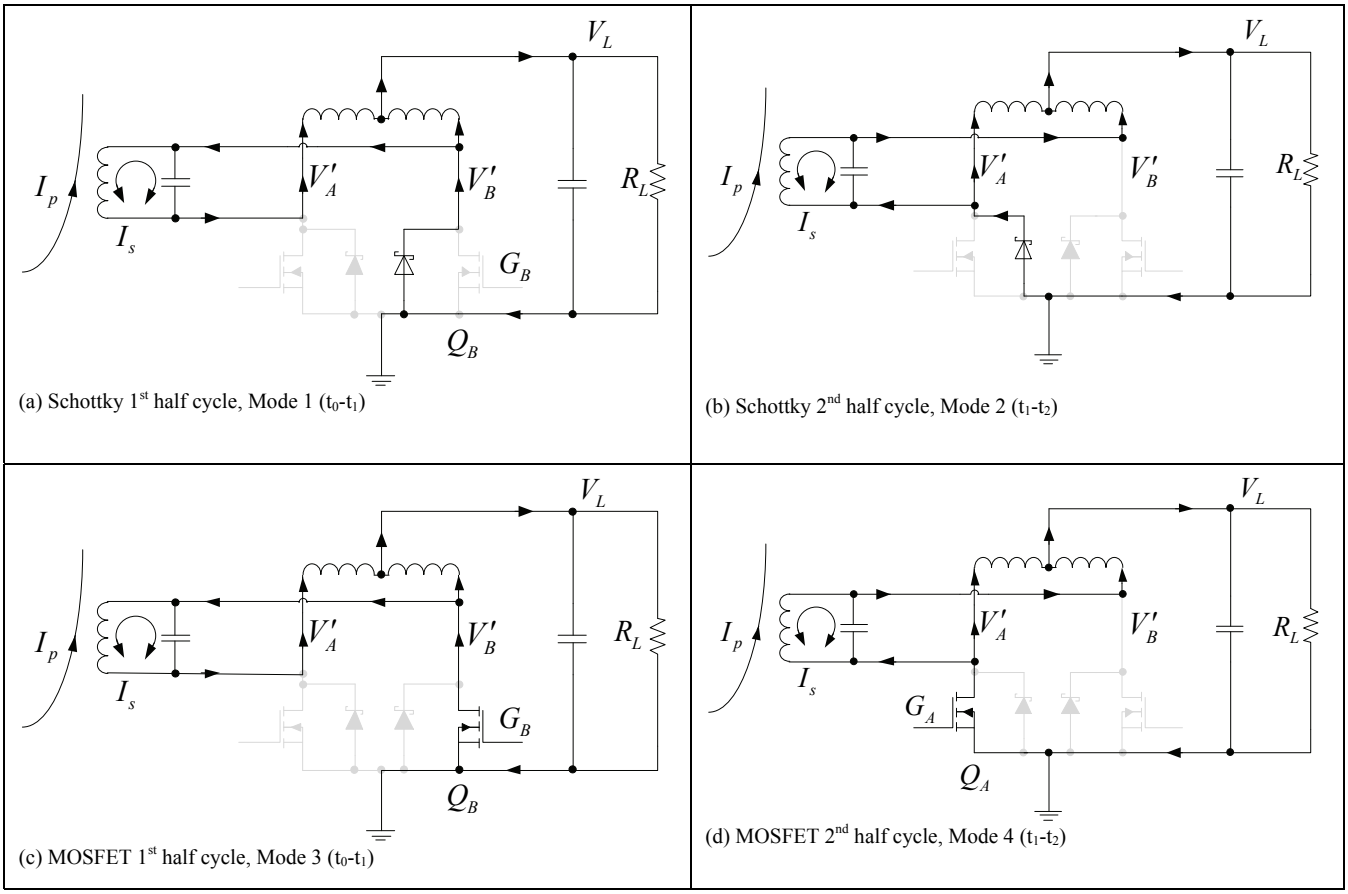

(a) Schottky 1st half cycle, Mode 1 (t_0-t_1)

(b) Schottky 2nd half cycle, Mode 2 (t_1-t_2)

(c) MOSFET 1st half cycle, Mode 3 (t_0-t_1)

(d) MOSFET 2nd half cycle, Mode 4 (t_1-t_2)

Fig. 2 During startup parallel Schottky diode operate to ramp up the heart pump load voltage as shown in (a) and (b), after sufficient voltage is present to power the gate drive circuitry the system transit to synchronous rectification using the MOSFETs as shown in (c) and (d).

II. Proposed Main Circuit Overview

Fig. 1 shows the main circuit of the proposed push-pull synchronous rectifier with the two passive Schottky diodes replaced with two active MOSFETs Q_A and Q_B. Two additional Schottky diodes are placed in parallel with the MOSFET body diodes to lower losses on startup and other MOSFET non-conduction periods. Because the proposed push-pull synchronous rectifier contains only low side MOSFETs, high side gate drives are not necessary. Such a synchronous rectifier is also named current doubler because the heart pump load current doubles that of average current through each MOSFET owing to the current addition of the two dc inductors at the positive terminal of the load.

III. Gate Drive Operation Analysis

Fig. 2 shows the circuit operation from startup to normal operation. On startup (Mode 1 and 2) the parallel Schottky diodes operate alternatively to increase the heart pump load voltage, once the load voltage reaches sufficient level for the drive options, the gate drive circuit then begins to operate the MOSFETs and the circuit now operates as a synchronous rectifier with commutating MOSFETs (Mode 3 and 4).

Fig. 3 and Fig. 4 show two different drive options for the MOSFETs in order to make it a synchronous rectifier. Both options employ the MOSFET drain to source voltages, V'_A and V'_B as the inputs and derive the gate drive signals from them. The passive autonomous rectifier feeds V'_A to a resistor and Zener to limit the voltage to the Zener voltage, a speed up capacitor is in parallel with the Zener resistance to give the right gate driving voltage G_B, similar action is applied to obtain G_A from V'_B.

The autonomous rectifier with the buffer circuit feeds V'_A through a resistor and Zener to limit V'_A to the Zener voltage and applies this voltage into a gate driver to generate G_B, a square wave for gate driving, similar action is applied to obtain G_A from V'_B.

Fig. 5 shows the theoretical waveforms for the passive autonomous synchronous rectifier. V'_A and V'_B are MOSFET drain to source voltages for MOSFETs Q_A and Q_B respectively. G_A and G_B are gate drive voltages for MOSFETs Q_A and Q_B respectively. During the first half cycle (Mode 3), G_B rises and falls with V'_A and is limited to the Zener voltage. G_B remains low with a low V'_A in the second half cycle (Mode 4). Similar detection approach and signal processing is applied to obtain G_A from V'_B.

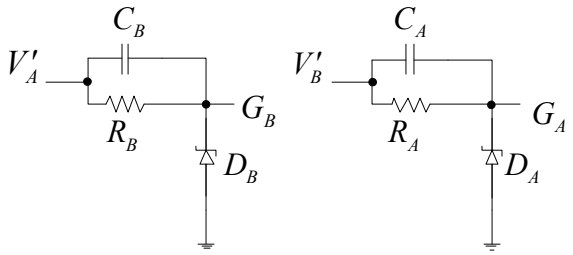

Fig. 3 Passive autonomous rectifier drive option

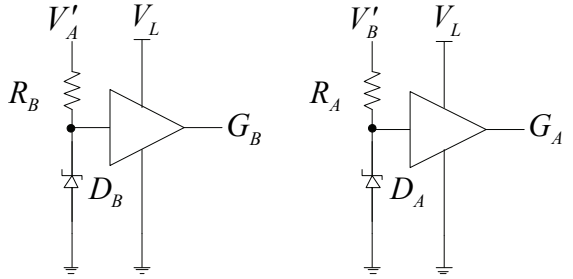

Fig. 4 Autonomous rectifier with buffer circuit drive option

The ideal gate drive waveforms are similar for the autonomous rectifier with buffer circuit synchronous rectifier as shown in Fig. 6, but the gate driving waveforms are squarer.

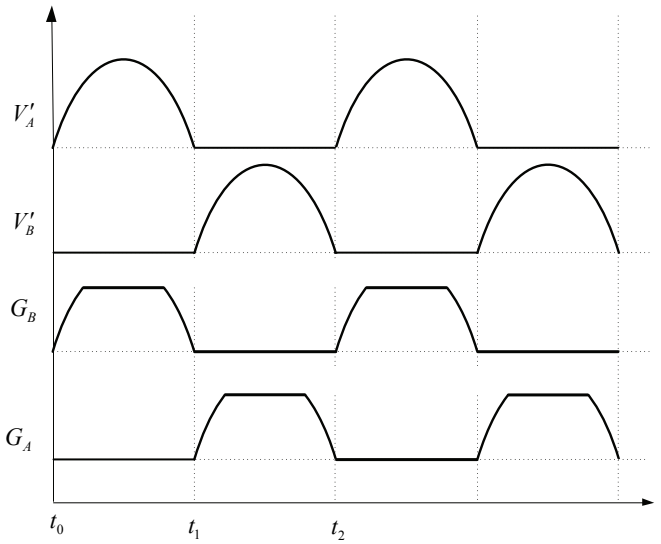

Fig. 5 Theoretical passive autonomous synchronous rectifier waveforms

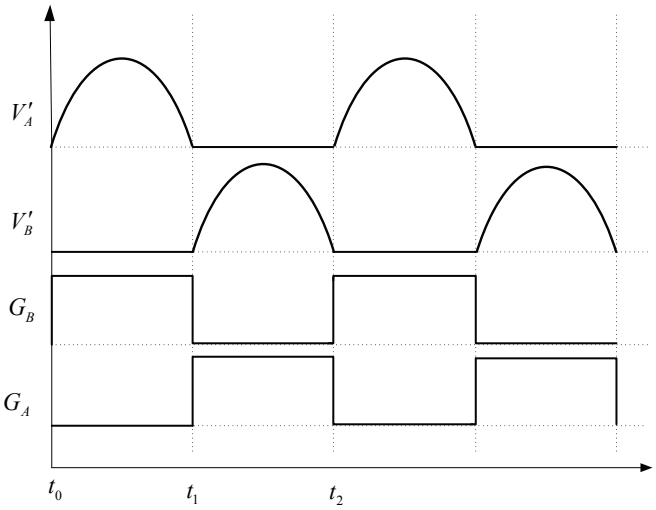

Fig. 6 Ideal gate drive waveform for autonomous rectifier with buffer circuit

$$\hat{v}_{ac} = \pi V_L \tag{1}$$

$$R_{eq} = \frac{\pi^2}{2} R_L \tag{2}$$

The relationship between resonant tank voltage peak and the heart pump load voltage is given by (1), and (2) gives the equivalent heart pump load seen by the secondary resonant tank.

IV. Circuit Design

Correct power rating components are selected for a 10V, 10Ω and 10W system. Here, a resistive load of 10Ω is used to model the practical operation of an implantable heart pump. To maximize efficiency, the synchronous MOSFETs are chosen to have a minimal total gate charge and ON-state resistance while withstanding the rated resonant voltage levels.

For the passive autonomous rectifier drive option, 10V Zener diodes are chosen to properly drive the MOSFETs. Zener saturation occurs when it is biased by at least 5mA (i_z), which depends on the difference between the ac peak given by (1) and the Zener voltage (V_z) as shown by (3). To improve the overall efficiency, the Zener bias resistor (R_Z) is chosen to be high (~1.2kΩ) to reduce power dissipation while sufficiently low to bias Zener correctly. This requires the speed up capacitor to be around 1nF to avoid erroneous and unstable gate drive waveforms during startup and system operation.

$$\frac{\hat{v}_{ac} - V_z}{R_z} > i_z \tag{3}$$

For the autonomous rectifier with buffer circuit, the same resistor and Zener setup is used before the gate driver. The ADP3624ARDZ gate driver is selected because it has a high switching speed and a high maximum single supply rating of

18V. The high maximum supply rating well exceeds the 10V rated load voltage and means the gate driver can be powered directly from the heart pump load voltage to remove the need of additional voltage regulators and its associated power losses.

The PCB board size is minimized to reduce noise through the use of surface mount components and tight component packing. Separate ground planes are used for signal and power in the autonomous rectifier with buffer circuit. The two ground planes are joined at the negative terminal of the heart pump load using a thicker track for power ground and a thinner track for signal ground. This attempts to avoid power ground currents affecting signal ground and its components.

A 1nF commutation capacitance can be placed close to the drains of two MOSFETs to reduce switching noise and the commutation loop formed by the capacitor and the two MOSFETs. However it does not necessarily lead to better efficiency due to added power losses inside the commutation capacitor.

TABLE I
SYSTEM PARAMETERS

Primary coil inductance (L_p)	11.3µH
Primary resonant capacitance (C_p)	47nF
Secondary coil inductance (L_s)	3.31µH
Secondary resonant capacitance (C_s)	220nF
Load resistance (R_L)	10Ω
System switching frequency (f_{sw})	178 kHz
Coil separation	5mm

V. SIMULATION AND EXPERIMENTAL RESULTS

The primary side or exterior circuitry is a current-fed parallel tuned push-pull converter, which is essentially the same circuit as the current doubler synchronous rectifier, but with reversed operation. The end-to-end efficiency measurements are done with the primary resonating at zero voltage switching (ZVS) frequency.

TABLE I provide parameters used to construct the system. Fig. 7 and Fig. 8 show the simulation waveforms for passive autonomous rectifier and autonomous rectifier with buffer circuit respectively. Fig. 9 shows the system experimental setup, it includes a primary converter, TET coils with adjustable coil separation distance, then the synchronous rectifier and resistive load. Fig. 10 and Fig. 11 show the oscilloscope waveforms for passive autonomous rectifier and autonomous rectifier with buffer circuit respectively. The simulation and experimental waveforms correspond well to each other.

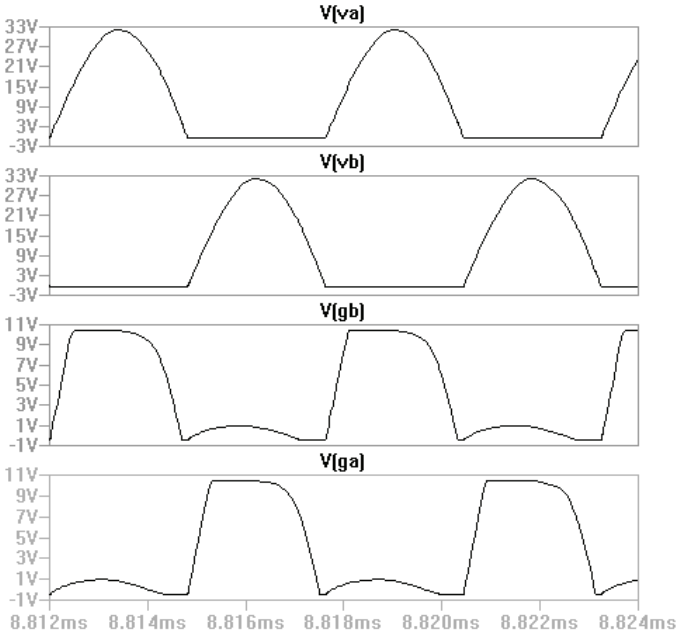

Fig. 7 Simulation waveform for passive autonomous synchronous rectifier

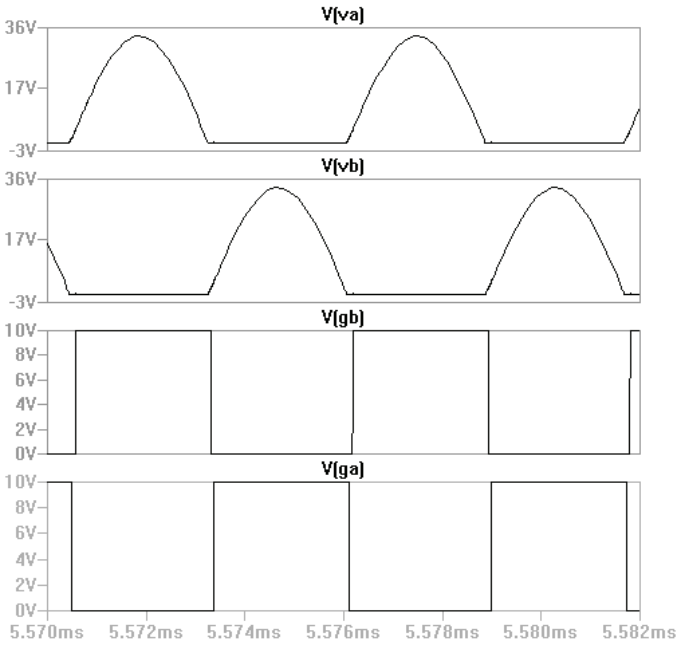

Fig. 8 Simulation waveform for autonomous rectifier with buffer circuit

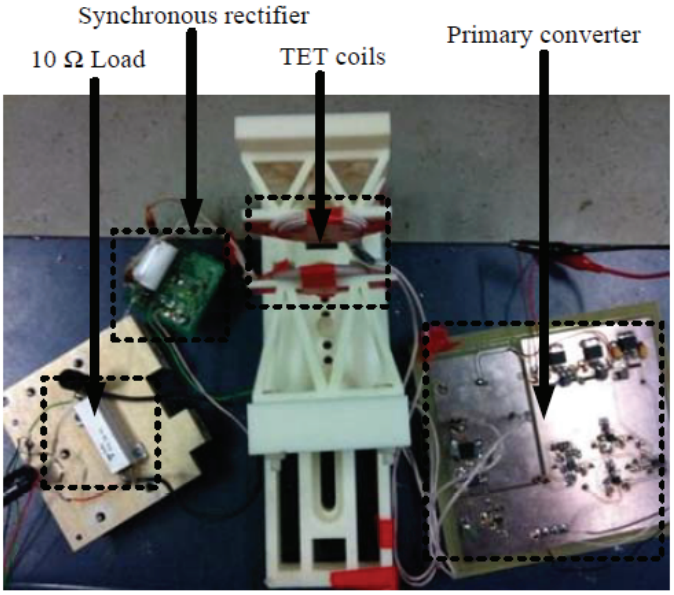

Fig. 9 Experimental Setup

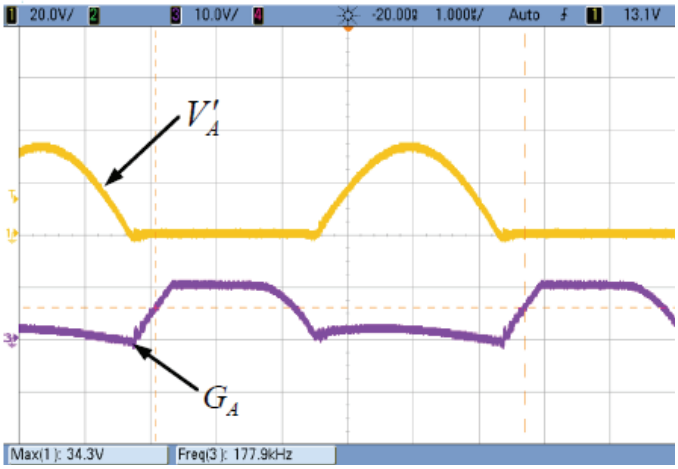

Fig. 10 Oscilloscope waveforms for passive autonomous synchronous rectifier

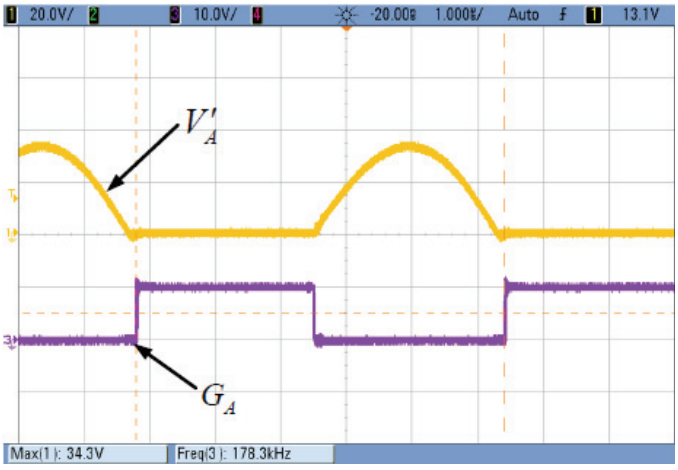

Fig. 11 Oscilloscope waveforms for autonomous rectifier with buffer circuit

The end-to-end power efficiency is measured when the coil separation is fixed at 5mm to keep the coupling coefficient constant. Under such a condition the ZVS frequency of the system is found to be 178 kHz. Fig. 12 shows the end-to-end efficiency against the output power delivered to the heart pump. These measurements are completed by incrementing the input voltage.

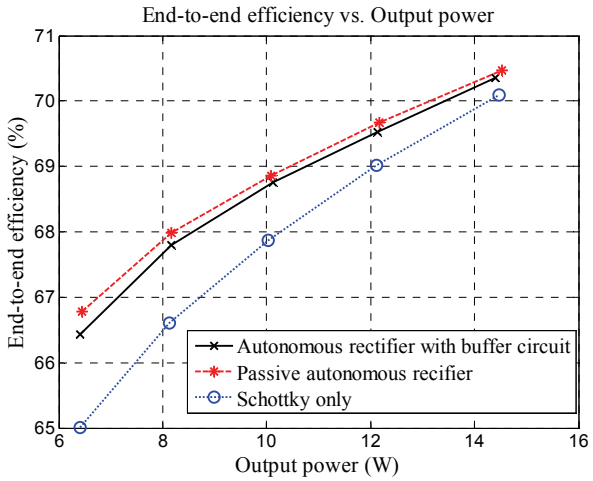

Fig. 12 End-to-end efficiency vs. output power for 5 mm coil separation

Fig. 12 shows that the two proposed drive options have achieved similar end-to-end efficiency, and that they are higher than the passive Schottky current doubler for the entire 6.4-14.4W measured range, including the 10W rated power for heart pump operation where the improvement is about 1.3%.

Fig. 12 also shows the end-to-end efficiency increases with the load power, P_L. This also increases the load current, ON state losses across commutating MOSFETs, ESR losses in dc inductors, resonant inductors and capacitors. However, the increase in load power (P_L) is higher than the increase in total power losses (P_{Loss}), so a higher overall end-to-end efficiency is achieved at higher power output according to the basic definition of end-to end power efficiency of the system given by (4).

$$\eta = \frac{P_L}{P_L + P_{Loss}} \times 100 \quad (4)$$

VI. Discussion

The passive autonomous synchronous rectifier has the benefit of a simple circuit without any auxiliary power supply; it also achieves similar end-to-end efficiencies compared to the autonomous rectifier with buffer circuit. However the passive autonomous synchronous rectifier may have frequency jittering and instability problems during startup and low resonant voltage operation. With quick startup processes and operation at a sufficiently high resonant voltage level, the system can reach stable steady state correctly.

The autonomous rectifier with a buffer circuit has a short delay time between commutations; this delay time is due to a minimum input voltage to toggle the gate driver ON. During the delay time both MOSFETs are off and parallel Schottky diodes would conduct to keep continuous current flow.

The experiment was conducted with an air gap. Given that

the permittivity of dry skin is not the same as that of air at the operating frequency [6], the corresponding efficiency result may be different. Therefore, further research with skin tissues will be needed for achieving practical transcutaneous energy transfer.

VII. CONCLUSIONS

This research has proposed and implemented an autonomous push-pull rectifier with passive or buffer circuit gate drives. The experimental results have demonstrated that the proposed synchronous rectifier can reduce the power losses of the implanted power pickup circuit and improve the overall end-to-end efficiency of the TET system for driving a 10W heart pump by 1.3% compared to the counterpart passive rectifier using Schottky diodes.

REFERENCES

[1] A. Danilov, G. Itkin, and S. Selishchev, "Progress in Methods for Transcutaneous Wireless Energy Supply to Implanted Ventricular Assist Devices," Biomedical Engineering, vol. 44, pp. 125-129, 2010.

[2] W. L. Holman, J. K. Kirklin, D. C. Naftel, R. L. Kormos, P. Desvign-Nickens, M. T. Camacho, et al., "Infection after implantation of pulsatile mechanical circulatory support devices," The Journal of Thoracic and Cardiovascular Surgery, vol. 139, pp. 1632-1636.e2, 2010.

[3] B. Wang, A. P. Hu, and D. M. Budgett, "Development of a push-pull current doubler synchronous rectifier for powering heart pumps," in Industrial Electronics and Applications (ICIEA), 2010 the 5th IEEE Conference on, 2010, pp. 1368-1372.

[4] H. Miura, S. Arai, Y. Kakubari, F. Sato, H. Matsuki, and T. Sato, "Improvement of the Transcutaneous Energy Transmission System Utilizing Ferrite Cored Coils for Artificial Hearts," Magnetics, IEEE Transactions on, vol. 42, pp. 3578-3580, 2006.

[5] H. Miura, S. Arai, F. Sato, H. Matsuki, and T. Sato, "A synchronous rectification using a digital PLL technique for contactless power supplies," Magnetics, IEEE Transactions on, vol. 41, pp. 3997-3999, 2005.

[6] IFAC. (2012). Calculation of the Dielectric Properties of Body Tissues in the frequency range 10 Hz - 100 GHz. Available: http://niremf.ifac.cnr.it/tissprop/htmlclie/htmlclie.htm